




Article

Facile Synthesis of Lacunary Keggin-Type Phosphotungstates-Decorated g-C₃N₄ Nanosheets for Enhancing Photocatalytic H₂ Generation

Na Lu ¹, Menghan Sun ¹, Xiaoming Wei ^{1,*}, Peng Zhang ² and Zhenyi Zhang ^{1,*}

¹ Key Laboratory of New Energy and Rare Earth Resource Utilization of State Ethnic Affairs Commission, Key Laboratory of Photosensitive Materials & Devices of Liaoning Province, School of Physics and Materials Engineering, Dalian Minzu University, 18 Liaohe West Road, Dalian 116600, China; luna@dlmu.edu.cn (N.L.); 18241113494@163.com (M.S.)

² School of Materials Science and Engineering, Zhengzhou University, Zhengzhou 450001, China; zhangp@zzu.edu.cn

* Correspondence: xmwei@dlmu.edu.cn (X.W.); zhangzy@dlmu.edu.cn (Z.Z.)

Received: 15 July 2020; Accepted: 25 August 2020; Published: 29 August 2020



Abstract: In this work, the lacunary Keggin-type phosphotungstates of [PW₉O₃₄]⁹⁻ (PW₉) clusters were loaded onto the g-C₃N₄ nanosheets (NSs) to synthesize the phosphotungstate clusters-decorated 2D heterojunction photocatalysts by using the electrostatic-force driven self-assembly process. The surface charge polarity of g-C₃N₄ NSs was changed from a negative to a positive charge through the acidizing treatment. The positively-charged g-C₃N₄ NSs allowed the negatively-charged PW₉ clusters to be adsorbed and deposited onto the g-C₃N₄ NSs, forming the PW₉/g-C₃N₄ heterojunction NSs. The as-synthesized samples were characterized by scanning electron microscopy (SEM), X-ray diffraction (XRD), Fourier-transform infrared (FTIR) spectroscopy, and UV-VIS absorption spectra, respectively. The photocatalytic activity tests indicated that, upon simulated sunlight irradiation, the photocatalytic H₂-generation rate of PW₉/g-C₃N₄ heterojunction NSs (~23.8 μmol h⁻¹) was ~3.3 times higher than that of the pure g-C₃N₄ NSs (~7.3 μmol h⁻¹). The enhanced photocatalytic activity of PW₉ cluster-decorated g-C₃N₄ NSs could be attributed to the enhanced separation process of the photoinduced charge-carriers, due to the Z-scheme-mediate charge transfer behavior across their hetero-interface.

Keywords: photocatalysis; g-C₃N₄; H₂ generation; Z-scheme mechanism; electron transfer

1. Introduction

The continuous burning of unsustainable fossil energy sources, which emits large amounts of harmful gases, has induced a global energy crisis and environmental contamination. The development of green renewable energy sources to replace traditional fossil energy sources has become an urgent issue [1,2]. As a kind of pollution-free sustainable fuel, hydrogen (H₂) has been regarded as an ideal candidate for the application of energy supply in future society [3,4]. Splitting water through the additional electric or photic energy is a common method to obtain the H₂. Since the H₂ generation from the photo-driven water splitting over the TiO₂ semiconductor photocatalyst was first reported in 1972 [5], this photochemical reaction has been widely used in the research area of solar-to-fuels conversion, mainly owing to its low cost and low energy consumption [6–8]. However, because the classical photocatalyst of TiO₂ nanostructures is a wide bandgap semiconductor (3.0–3.2 eV), it can only absorb the UV light that accounts for 3–5% in the solar spectrum [9,10]. Thus, the development of narrow bandgap semiconductors as the photocatalysts for H₂ generation has emerged as a hot topic in the area of solar-to-fuels conversion.

As a polymeric semiconductor made of carbon and nitrogen elements, graphite C_3N_4 (g- C_3N_4) material has attracted increasing interest in the area of photocatalytic H_2 generation [11,12]. This kind of metal-free semiconductor with a 2D nanosheet structure can open new prospects for the application of solar-to-fuels conversion because it is an abundant, cheap and stable semiconductor, with a suitable energy-level position for reducing protons. However, the fast recombination of the photoinduced charge-carriers often results in poor photocatalytic activity of the g- C_3N_4 NSs [13]. To overcome this problem, much effort has been contributed to couple the g- C_3N_4 NSs with an appropriate photoactive material to construct the 2D heterojunction photocatalyst toward high-efficient photocatalytic H_2 generation.

As a class of polyoxometalates, lacunary Keggin-type phosphotungstates have been extensively investigated as photosensitizers for enhancing the photocatalytic activity of the semiconductor photocatalysts for H_2O_2 production, H_2 generation, CO_2 reduction, pollution degradation, and organic material synthesis [14–16]. Similar to the inorganic semiconductors, the phosphotungstates also have the photoinduced electron transition behavior from the HOMO (Highest Occupied Molecular Orbital) to LUMO (Lowest Unoccupied Molecular Orbital). In general, the charge-transfer from the ligand to metal (O to W) in the phosphotungstates enable them to possess a high light absorption coefficient. Meanwhile, the enriched metal nodes of such W in the phosphotungstates can boost the photoinduced multi-electron redox-processes for fulfilling the various photo-chemical reactions [17]. Furthermore, when the lacunary Keggin-type phosphotungstates are dissolved in a water solution, the negatively-charged phosphotungstates can be obtained due to the ionization effect, thereby leading the phosphotungstates to be easily absorbed onto the substrate with the positive charge [18,19]. Notably, the surface charge polarity of g- C_3N_4 NSs is controllable by the acidizing treatment. It is concluded that the lacunary Keggin-type phosphotungstates are one of the ideal guest photosensitizers for coupling with the g- C_3N_4 NSs host, through the electrostatic-force driven self-assembly process for enhancing the photocatalytic H_2 generation of g- C_3N_4 NSs.

In this work, we adjusted the surface charge polarity of g- C_3N_4 to positive by using the acidizing treatment, and loaded the lacunary Keggin-type phosphotungstates of $[PW_9O_{34}]^{9-}$ (PW_9) clusters onto the g- C_3N_4 NSs, forming the $PW_9/g-C_3N_4$ heterojunction NSs, via a facile self-assembly process due to the electrostatic interaction. We expected to utilize the photoinduced electrons on the LUMO of PW_9 component transfer to the valence band (VB) of g- C_3N_4 component for extending the lifetime of photoinduced electrons on the conduction band (CB) of g- C_3N_4 for executing protons reduction and improving the photocatalytic activity of the $PW_9/g-C_3N_4$ heterojunction NSs for H_2 generation. It is believed that our work will provide a new platform to construct the ultra-small polyoxometalates cluster-decorated g- C_3N_4 NSs for highly-efficient photocatalytic solar-to-fuels conversion.

2. Experimental

2.1. Synthesis of the PW_9 , g- C_3N_4 NS, and $PW_9/g-C_3N_4$ Heterojunction NSs

The lacunary Keggin-type phosphotungstates of $Na_9[A-\alpha-PW_9O_{34}] \cdot 7H_2O$ (named as PW_9) were synthesized by using the previously reported method [20]. The g- C_3N_4 was synthesized through the traditional thermal polymerization method by using the urea as the precursor [21]. To obtain the $PW_9/g-C_3N_4$ heterojunction NSs, 100 mg of the g- C_3N_4 bulk was ground and then dispersed into deionized water under the ultrasonic treatment for 90 min at room temperature, thereby achieving the g- C_3N_4 nanosheets (NSs). Afterward, 1 M of HCl solution was added dropwise into the above g- C_3N_4 nanosheets-suspended water solution to adjust the surface charge polarity of the NSs. After that, 100 mg of the PW_9 was dissolved into the above solution with vigorous stirring for 4 h. The precipitate in the solution was separated by centrifugation treatment. Finally, the obtained mixture was dried at 80 °C for 12 h, which was then under annealing at 300 °C for 2 h in vacuum. Thus, the $PW_9/g-C_3N_4$ heterojunction NSs were synthesized.

2.2. Characterization

The structure and morphology of the as-synthesized samples were observed by scanning electron microscopy (Field Emission-SEM; S-4800, Hitachi, Tokyo, Japan) and transmission electron microscopy (TEM) (JEM-2100, JEOL, Tokyo, Japan). The X-ray diffraction (XRD) patterns of the as-fabricated samples were studied by X-ray diffractometer (XRD-6000, Shimadzu, Tokyo, Japan) with a Cu K α line of 0.1541 nm and the radiation is from 10° to 65° at a scanning rate at 2°/min. The Fourier-transform infrared (FTIR) spectra were recorded on Magna 560 FTIR spectrometer (Thermo Nicolet Corporation, Madison, WI, USA) with a resolution of 1 cm⁻¹. The UV-VIS absorption spectra of the samples were recorded on a Lambda 750 UV/VIS/NIR spectrophotometer (Perkin Elmer, Waltham, MA, USA). The specific surface areas of the as-prepared samples were measured with a Micromeritics ASAP-2020 instrument (USA), and analyzed by the Brunauer–Emmett–Teller (BET) method. The surface charge polarity of the samples was measured with a dynamic light scattering spectrophotometer and isoelectric point determination with zeta potential analysis (SZ-100, Horiba, Tokyo, Japan).

2.3. Photocatalytic H₂ Generation

Five milligrams of the as-synthesized samples were dispersed into 10 mL of a water solution containing triethanolamine (TEOA, 15 vol.%) and chloroplatinic acid (H₂PtCl₆, 10 μ L, 12 mM). Then, the mixture solution was sealed in a quartz reactor and then ventilated with argon gas for 10 min to drive away the residual air. Afterward, the reactor was exposed under simulated sunlight (300-W Xe lamp, PLS-SXE300UV, Beijing, China, coupled with an AM 1.5 filter, the wavelength range of light was from 320–2500 nm, the light density was 100 mW cm⁻², and the photon flux of the lamp was 0.17 μ mol s⁻¹ m⁻²). The produced gas was periodically analyzed by a gas chromatograph (GC) equipped with a thermal conductivity detector (TCD) (Beifen-Ruili Analytical Instrument, SP-3420A, Beijing, China).

3. Results and Discussion

To synthesize the PW₉/g-C₃N₄ heterojunction NSs, the g-C₃N₄ bulk was crushed into the g-C₃N₄ nanosheets (NSs), at first, through the ultrasonic method. Then the obtained g-C₃N₄ NSs underwent the acidizing treatment to adjust their surface charge polarity from -21 mV to +6.6 mV. Afterward, the positively-charged g-C₃N₄ NSs were suspended into the water solution of PW₉ to enable the negatively-charged PW₉ to be self-assembled onto the g-C₃N₄ NSs, based on the electrostatic force [22,23]. Finally, the target sample of PW₉/g-C₃N₄ heterojunction NSs was synthesized for further investigation. Figure 1B shows the scanning electron microscopy (SEM) image of the pure g-C₃N₄ NSs. It can be seen that the sheet-like g-C₃N₄ has a relatively smooth surface. After PW₉ loading, there was also no change on the surface roughness of the g-C₃N₄ NSs in the PW₉/g-C₃N₄ composite NSs (Figure 1C). In order to further investigate the as-prepared PW₉/g-C₃N₄ heterojunction NSs, the high-resolution transmission electron microscopy (HRTEM) and the dark-filed scanning mode TEM were carried out. Although the lattice-fringe spacing of both PW₉ and g-C₃N₄ cannot be observed in HRTEM (Figure 1D), further investigation, by using dark-filed scanning mode TEM (STEM), indicated that the PW₉ clusters with sizes of 3–5 nm were decorated on the surface of g-C₃N₄ NSs in their heterojunction NSs (Figure 1E). In addition, the specific surface areas of PW₉/g-C₃N₄ heterojunction NSs (~68.7 m²/g) was similar to that of g-C₃N₄ (~53.1 m²/g), as shown in Figure S1.

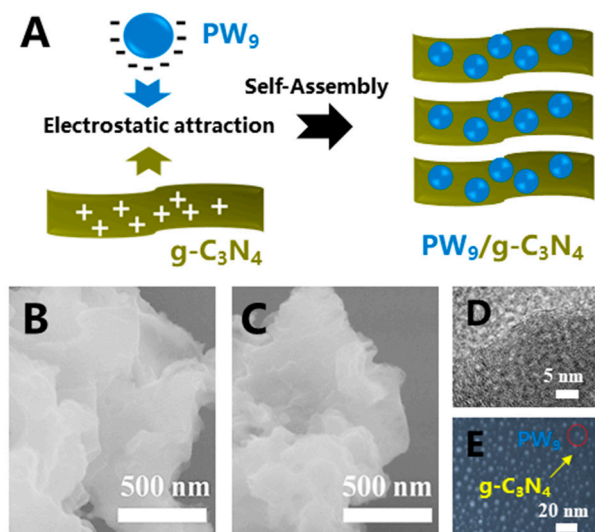


Figure 1. (A) Schematic diagram of the self-assembly process of the $\text{PW}_9/\text{g-C}_3\text{N}_4$ heterojunction NSs, based on the electrostatic force between these two hetero-components; SEM images of (B) $\text{g-C}_3\text{N}_4$ NSs and (C) $\text{PW}_9/\text{g-C}_3\text{N}_4$ heterojunction NSs; the HRTEM image (D) and the dark-field STEM image (E) of the heterojunction NSs.

The phase structures of the as-synthesized samples were identified through X-ray diffraction (XRD) patterns. As shown in Figure 2, the two intense diffraction peaks around $28^\circ\sim 30^\circ$ can be observed on the XRD pattern of the PW_9 , which is in accordance with the feature peaks of the PW_9 reported in the literature [24]. Meanwhile, the other peaks on the diffraction pattern of the Na-PW_9 were also matched with that of the reported PW_9 , confirming the obtained lacunary Keggin-type phosphotungstates of PW_9 . In the case of $\text{g-C}_3\text{N}_4$ NSs, the two feature diffraction peaks, belonging to the periodic structure of intra-planar tri-s-triazine and the interlayer stacking of conjugated aromatic structures of $\text{g-C}_3\text{N}_4$ NSs were found at 13.1° and 27.4° , respectively [25–28]. This is in agreement with the graphite structure of carbon nitride. When the modification of $\text{g-C}_3\text{N}_4$ NSs with PW_9 clusters took place, the feature peaks originated from the Na-PW_9 with the center at 29.3° and the $\text{g-C}_3\text{N}_4$ NSs with centers at 13.1° and 27.4° and appeared on the XRD pattern of the formed composite. This result suggests that the $\text{g-C}_3\text{N}_4$ NSs were decorated with the lacunary Keggin-type phosphotungstates of PW_9 clusters.

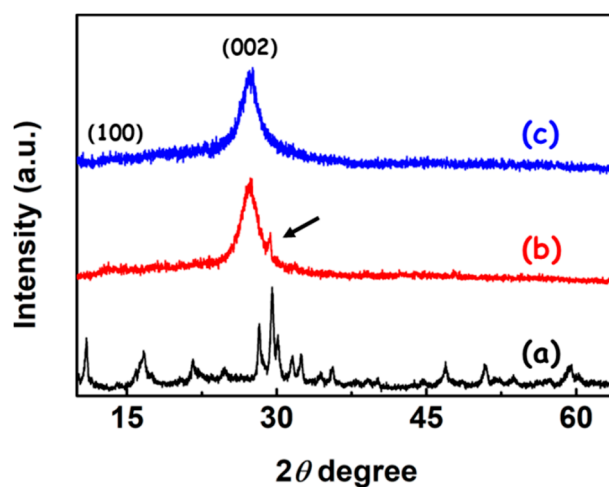


Figure 2. XRD patterns of the as-synthesized samples: (a) PW_9 ; (b) $\text{PW}_9/\text{g-C}_3\text{N}_4$ heterojunction NSs; (c) $\text{g-C}_3\text{N}_4$ NSs.

To further confirm the existence of the PW_9 clusters on the $g-C_3N_4$ NSs, the Fourier-transform infrared (FTIR) spectra of the $PW_9/g-C_3N_4$ heterojunction NSs along with the corresponding single hetero-components were tested, as shown in Figure 3. For the pure PW_9 , the classical stretching vibrations related to the W-O-W, W-O, and P-O bonds were positioned around the 804/890, 984, and 1077 cm^{-1} , respectively [29,30]. It further proves the formation of lacunary Keggin-type phosphotungstates of PW_9 . In the case of pure $g-C_3N_4$ NSs, the vibration bands between 1200 and 1650 cm^{-1} were ascribed to the CN heterocycles [24,31]. The band at 811 cm^{-1} is attributed to the feature vibration mode of s-triazine ring unit [32]. These observations are consistent with the literatures. The feature stretching vibration bands of both PW_9 and $g-C_3N_4$ could be found on the FTIR spectrum of the $PW_9/g-C_3N_4$ heterojunction NSs, powerfully confirming the successful decoration of the PW_9 clusters onto the $g-C_3N_4$ NSs. Notably, as compared with pure $g-C_3N_4$, the feature band at 811 cm^{-1} was slightly shifted to 809 cm^{-1} , which might be the cause of the chemical interaction between PW_9 and $g-C_3N_4$ produced by the electrostatic adsorption process.

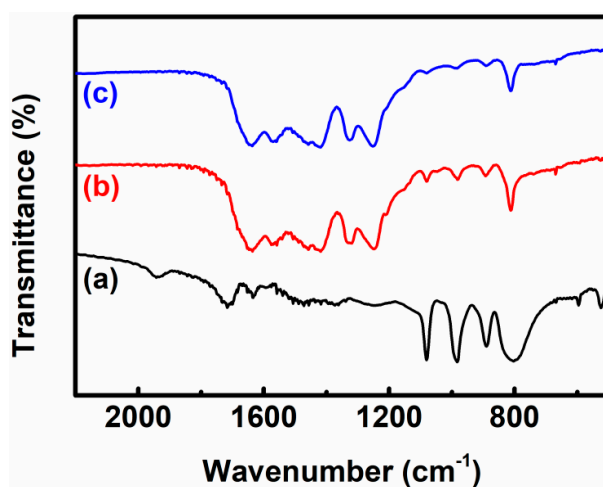


Figure 3. FTIR spectra of the as-synthesized samples: (a) PW_9 ; (b) $PW_9/g-C_3N_4$ heterojunction NSs; (c) $g-C_3N_4$ NSs.

The light absorption behaviors of the as-synthesized samples were evaluated through UV-VIS absorption spectra. As observed in Figure 4, the absorption edge of the pure PW_9 is located around 350 nm, corresponding to the forbidden gap of ~ 3.5 eV between HOMO and LUMO of the PW_9 [15,33]. Meanwhile, the absorption edge of pure $g-C_3N_4$ NSs appears at ~ 480 nm, suggesting the ~ 2.6 eV of the bandgap of the $g-C_3N_4$ NSs [34]. The above results indicate that the PW_9 and $g-C_3N_4$ NSs are the UV and visible absorbers, respectively, during the photo-excitation process. After loading the PW_9 clusters onto the surface of $g-C_3N_4$ NSs, the formed $PW_9/g-C_3N_4$ heterojunction NSs displayed the blue-shift behavior of the absorption edge, due to the introduction of the UV-light-active PW_9 hetero-component. By combining the results of the SEM, TEM, XRD, FTIR, and UV-VIS absorption spectra, we confirm that the $PW_9/g-C_3N_4$ heterojunction NSs with a well-distribution of PW_9 clusters were successfully synthesized by using the self-assembly process driven by the electrostatic force.

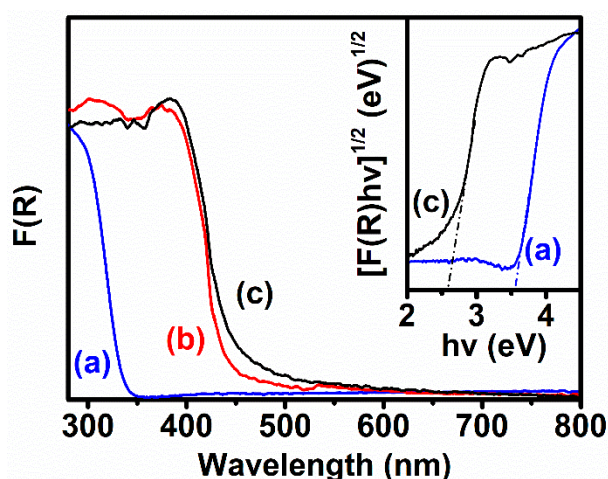


Figure 4. UV-VIS absorption spectra of the as-synthesized samples: (a) PW₉; (b) PW₉/g-C₃N₄ heterojunction NSs; (c) g-C₃N₄ NSs; the inset were plots of the $[F(R)hv]^{1/2}$ versus $h\nu$ of (a) PW₉; (c) g-C₃N₄ NSs.

Photocatalytic activity of the as-synthesized PW₉/g-C₃N₄ heterojunction NSs for H₂ generation was assessed under simulated sunlight excitation in the presence of the sacrificial agent of triethanolamine (TEOA) to quench the photoinduced hole. As observed in Figure 5A, there is no observable H₂ generation under simulated sunlight irradiation for 2 h, when using the single PW₉ as the photocatalyst. Meanwhile, the pure g-C₃N₄ NSs only displayed a poor photocatalytic activity for H₂ generation (~14.6 μmol in 2 h-irradiation). After self-assembling the PW₉ clusters onto the g-C₃N₄ NSs to form the PW₉/g-C₃N₄ heterojunction NSs, the photocatalytic activity of the heterojunction NSs for H₂ generation remarkably increased to ~47.6 μmol in 2 h-irradiation. The H₂ generation rate of the PW₉/g-C₃N₄ heterojunction NSs was 3.3 times higher than that of the g-C₃N₄ NSs, as summarized in Figure 5B. Notably, this photocatalytic activity is almost the highest one among the values reported for other g-C₃N₄-based photocatalytic systems (Table 1). Moreover, the solar-to-hydrogen (STH) efficiency has become an important index for evaluating the photocatalytic activity of hydrogen production. The STH efficiency under simulated sunlight irradiation can be calculated according to the following equation [35,36]:

$$\text{STH} = \frac{\text{Energy of generation of hydrogen by water splitting}}{\text{Solar energy irradiating the reaction cell}} \times 100\% \quad (1)$$

After calculating, the STH of PW₉/g-C₃N₄ heterojunction NSs was determined to be about 0.26% at room temperature.

It should be pointed out that the LUMO potential of PW₉ does not satisfy the demand of proton reduction, while the g-C₃N₄ possesses a suitable conduction band (CB) potential for fulfilling the H₂ generation [37,38]. Thus, we could deduce that the photocatalytic sites in the PW₉/g-C₃N₄ heterojunction NSs should be located at the surface of g-C₃N₄ hetero-component [39,40]. Meanwhile, the PW₉ hetero-component serves as the photosensitizer to boost the separation process of the photoinduced charge-carriers of the g-C₃N₄ hetero-component. According to the energy band structures of the reported Keggin-type phosphotungstates and g-C₃N₄ NSs, the LUMO position is a little higher than the valence band (VB) position of the g-C₃N₄ NSs, as illustrated in the inset of Figure 5B. Thus, when the PW₉/g-C₃N₄ heterojunction NSs is excited by simulated sunlight that contains the photon energies in both UV and visible light regions, the photoinduced electron-hole pairs are generated on the LUMO and VB of the PW₉ and g-C₃N₄ hetero-components, respectively [41,42]. Owing to the potential difference between the LUMO of PW₉ and the VB of g-C₃N₄, the photoinduced electrons on the LUMO of PW₉ could transfer to the VB of g-C₃N₄ in the heterojunction NSs, thereby extending the lifetimes of the photoinduced electrons on the CB of g-C₃N₄ for implementing the photocatalytic H₂

generation [43]. In this way, the Z-scheme photocatalytic mechanism can be employed to explain the enhanced photocatalytic activity of the $\text{PW}_9/\text{g-C}_3\text{N}_4$ heterojunction system.

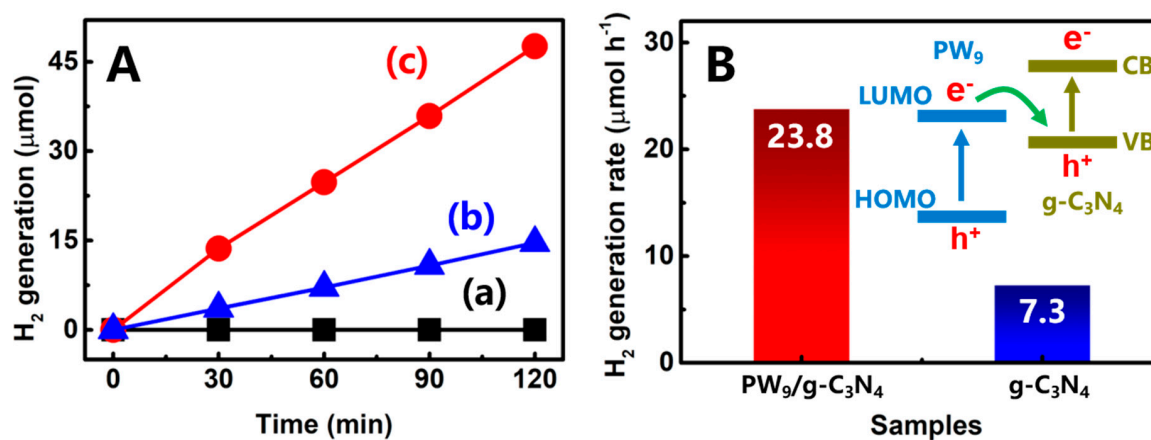


Figure 5. (A) Time-dependent photocatalytic H₂-generation plots over the different samples under simulated sunlight irradiation: (a) PW₉; (b) g-C₃N₄ NSs; (c) PW₉/g-C₃N₄ heterojunction NSs; (B) H₂-generation rates of the PW₉/g-C₃N₄ heterojunction and g-C₃N₄ NSs.

Table 1. Photocatalytic activity of reported g-C₃N₄-based photocatalysts for H₂ evolution.

Catalyst	Precursor	Light Source	Activity	Ref.
Ag/g-C ₃ N ₄ /TiO ₂	Melamine	300 W Xe lamp with AM 1.5 filter	1.5 μmol/h	[44]
W ₁₈ O ₄₉ /g-C ₃ N ₄	Urea	300 W Xe lamp with λ > 420 nm filter	3.69 μmol/h	[45]
g-C ₃ N ₄ /MnO ₂	Urea	300 W Xe lamp with λ > 420 nm filter	5.53 μmol/h	[46]
ZnIn ₂ S ₄ /g-C ₃ N ₄	Melamine	300 W Xe lamp with λ > 420 nm filter	14.1 μmol/h	[47]
W ₁₈ O ₄₉ /g-C ₃ N ₄	Melamine	300 W Xe lamp with λ > 420 nm filter	18.25 μmol/h	[48]
Zn-AgIn ₅ S ₈ /g-C ₃ N ₄	Urea	300 W Xe lamp with λ > 420 nm filter	17.32 μmol/h	[49]
MoS ₂ /g-C ₃ N ₄	Urea	300 W Xe lamp with λ > 420 nm filter	19.66 μmol/h	[50]
PW ₉ /g-C ₃ N ₄	Urea	300 W Xe lamp with AM 1.5 filter	23.8 μmol/h	This work

If the Z-scheme electron-transfer process is the main factor for enhancing the photocatalytic activity of $\text{PW}_9/\text{g-C}_3\text{N}_4$ heterojunction NSs, the hetero-interface combination force between these two hetero-components should have an influence on the photocatalytic H₂ generation of the NSs. In order to investigate this hypothesis, we synthesized another heterojunction NSs of g-C₃N₄, decorated with the normal Keggin-type phosphotungstic acid ($\text{H}_3\text{PW}_{12}\text{O}_{40}$) (PW_{12}). Because the number of the negative charges in PW_{12} is less than that in PW_9 when dissolving them in water solution, the combination force between the PW_{12} and g-C₃N₄ should be lower than that in the PW_9 and g-C₃N₄ system. In theory, a strong combination force between the hetero-components would build a high-quality of the transport channel for electron transfer between the hetero-components [51,52]. Thus, the interfacial electron transfer process in the $\text{PW}_9/\text{g-C}_3\text{N}_4$ heterojunction NSs should be more effective for driving the Z-scheme photocatalytic H₂ generation as compared to the $\text{PW}_{12}/\text{g-C}_3\text{N}_4$ heterojunction NSs (the insets of Figure 6) [53]. The comparison study of the photocatalytic activities of the above two heterojunction NSs indicated that the H₂-generation activity of $\text{PW}_9/\text{g-C}_3\text{N}_4$ heterojunction NSs (~47.6 μmol in 2 h irradiation) was ~1.3 times higher than that of the $\text{PW}_{12}/\text{g-C}_3\text{N}_4$ heterojunction NSs (~35.3 μmol in 2 h irradiation). This evidence further confirms a fast Z-scheme charge-transfer process occurred in the intimate hetero-interface of $\text{PW}_9/\text{g-C}_3\text{N}_4$ for enhancing the photocatalytic H₂ generation.

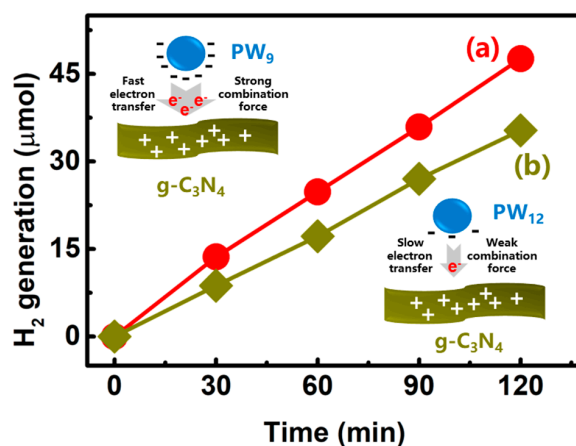


Figure 6. Time-dependent photocatalytic H₂-generation plots over (a) PW₉/g-C₃N₄ heterojunction NSs and (b) PW₁₂/g-C₃N₄ heterojunction NSs upon simulated sunlight irradiation. The insets showing the interfacial adsorption and electron transfer abilities of the PW₉/g-C₃N₄ heterojunction and PW₁₂/g-C₃N₄ heterojunction NSs.

4. Conclusions

In summary, the lacunary Keggin-type phosphotungstates/g-C₃N₄ heterojunction NSs were synthesized through self-assembling the PW₉ clusters onto the g-C₃N₄ NSs, based on the electrostatic adsorption process. When adjusting the surface charge polarity of g-C₃N₄ NSs from the negative to the positive charge in the PW₉-dissolved solution, it was found that the intimate hetero-interface between PW₉/g-C₃N₄ heterojunction NSs could be built for boosting the Z-scheme charge-transfer process. Upon simulated sunlight irradiation, the lifetimes of the photoinduced electrons on the g-C₃N₄ hetero-component were prolonged in the heterojunction NSs. Thus, a ~3.3-fold enhancement of the photocatalytic activity for H₂ generation was observed over the PW₉/g-C₃N₄ heterojunction NSs as compared to the pure g-C₃N₄ NSs. Our work will provide a new platform to construct the ultra-small sized polyoxometalates clusters-based Z-scheme photocatalysts for enhancing the photocatalytic solar-to-fuels conversion.

Supplementary Materials: The following are available online at <http://www.mdpi.com/2073-4360/12/9/1961/s1>, Figure S1: Nitrogen adsorption-desorption isotherms of the as-synthesized samples: (a) g-C₃N₄, (b) PW₉/g-C₃N₄ heterojunction NSs.

Author Contributions: Conceptualization, N.L. and Z.Z.; methodology, N.L. and M.S.; data curation, N.L. and M.S.; funding acquisition, N.L. and Z.Z.; investigation, Z.Z. and P.Z.; supervision, Z.Z. and X.W.; validation, N.L. and M.S.; visualization, N.L. and P.Z.; writing—original draft, N.L. and X.W.; writing—review and editing, N.L. and Z.Z. All authors have read and agreed to the published version of the manuscript.

Funding: This work is supported by the National Natural Science Foundation of China (Grant No. 51872068, 51772041), the Natural Science Foundation of Liaoning Province (Grant No. 2017054190), the Program for Dalian Excellent Talents (Grant No. 2016RQ069), the Program for Liaoning Excellent Talents in University (LNET) (Grant No. LR2017004), Liaoning Revitalization Talents Program (Grant No. XLYC1807176), Educational Committee Foundation of Liaoning Province (Grant No. LJYT201907), the Natural Science Foundation of Liaoning Province (Grant No. 2020-MZLH-15), and Dalian Science Foundation for Distinguished Young Scholars (Grant No. 2018RJ05). Zhenyi Zhang acknowledges the support from the Liaoning BaiQianWan Talents Program.

Conflicts of Interest: The authors declare no conflict of interest.

References

- Liu, J.; Liu, Y.; Liu, N.; Han, Y.; Zhang, X.; Huang, H.; Lifshitz, Y.; Lee, S.-T.; Zhong, J.; Kang, Z. Metal-free efficient photocatalyst for stable visible water splitting via a two-electron pathway. *Science* **2015**, *347*, 970–974. [[CrossRef](#)] [[PubMed](#)]
- Cao, S.; Low, J.; Yu, J.; Jaroniec, M. Polymeric Photocatalysts Based on Graphitic Carbon Nitride. *Adv. Mater.* **2015**, *27*, 2150–2176. [[CrossRef](#)] [[PubMed](#)]

3. Amirav, L.; Alivisatos, A.P. Photocatalytic Hydrogen Production with Tunable Nanorod Heterostructures. *J. Phys. Chem. Lett.* **2010**, *1*, 1051–1054. [[CrossRef](#)]
4. Bai, Y.; Wilbraham, L.; Slater, B.J.; Zwijnenburg, M.A.; Sprick, R.S.; Cooper, A.I. Accelerated Discovery of Organic Polymer Photocatalysts for Hydrogen Evolution from Water through the Integration of Experiment and Theory. *J. Am. Chem. Soc.* **2019**, *141*, 9063–9071. [[CrossRef](#)]
5. Fujishima, A.; Honda, K. Electrochemical photolysis of water at a semiconductor electrode. *Nature* **1972**, *238*, 37–38. [[CrossRef](#)]
6. Gul, I.; Sayed, M.; Shah, N.S.; Ali Khan, J.; Polychronopoulou, K.; Iqbal, J.; Rehman, F. Solar light responsive bismuth doped titania with Ti^{3+} for efficient photocatalytic degradation of flumequine: Synergistic role of peroxy monosulfate. *Chem. Eng. J.* **2020**, *384*, 123255. [[CrossRef](#)]
7. Sayed, M.; Arooj, A.; Shah, N.S.; Khan, J.A.; Shah, L.A.; Rehman, F.; Arandiyani, H.; Khan, A.M.; Khan, A.R. Narrowing the band gap of TiO_2 by co-doping with Mn^{2+} and Co^{2+} for efficient photocatalytic degradation of enoxacin and its additional peroxidase like activity: A mechanistic approach. *J. Mol. Liq.* **2018**, *272*, 403–412. [[CrossRef](#)]
8. Sayed, M.; Gul, M.; Shah, N.S.; Khan, J.A.; Khan, Z.U.H.; Rehman, F.; Khan, A.R.; Rauf, S.; Arandiyani, H.; Yang, C.P. In-situ dual applications of ionic liquid coated Co^{2+} and Fe^{3+} co-doped TiO_2 : Superior photocatalytic degradation of ofloxacin at pilot scale level and enhanced peroxidase like activity for calorimetric biosensing. *J. Mol. Liq.* **2019**, *282*, 275–285. [[CrossRef](#)]
9. Chen, X.; Mao, S.S. Titanium dioxide nanomaterials: Synthesis, properties, modifications, and applications. *Chem. Rev.* **2007**, *107*, 2891–2959. [[CrossRef](#)]
10. Chiarello, G.L.; Dozzi, M.V.; Selli, E. TiO_2 -based materials for photocatalytic hydrogen production. *J. Energy Chem.* **2017**, *26*, 250–258. [[CrossRef](#)]
11. Cao, S.; Yu, J. g- C_3N_4 -Based Photocatalysts for Hydrogen Generation. *J. Phys. Chem. Lett.* **2014**, *5*, 2101–2107. [[CrossRef](#)] [[PubMed](#)]
12. He, F.; Wang, Z.; Li, Y.; Peng, S.; Liu, B. The nonmetal modulation of composition and morphology of g- C_3N_4 -based photocatalysts. *Appl. Catal. B Environ.* **2020**, *269*. [[CrossRef](#)]
13. Hu, C.; Lin, Y.-R.; Yang, H.-C. Recent Developments in Graphitic Carbon Nitride Based Hydrogels as Photocatalysts. *ChemSusChem* **2019**, *12*, 1794–1806. [[CrossRef](#)] [[PubMed](#)]
14. Balula, S.S.; Santos, I.C.M.S.; Cunha-Silva, L.; Carvalho, A.P.; Pires, J.; Freire, C.; Cavaleiro, J.A.S.; de Castro, B.; Cavaleiro, A.M.V. Phosphotungstates as catalysts for monoterpenes oxidation: Homo- and heterogeneous performance. *Catal. Today* **2013**, *203*, 95–102. [[CrossRef](#)]
15. Meng, J.; Wang, X.; Yang, X.; Hu, A.; Guo, Y.; Yang, Y. Enhanced gas-phase photocatalytic removal of aromatics over direct Z-scheme-dictated $H_3PW_{12}O_{40}/g-C_3N_4$ film-coated optical fibers. *Appl. Catal. B Environ.* **2019**, *251*, 168–180. [[CrossRef](#)]
16. Wang, Y.; Liu, J.; Wang, Y.; Zhang, M. CO_2 photoreduction to CO/CH_4 over $Bi_2W_{0.5}Mo_{0.5}O_6$ solid solution nanotubes under visible light. *RSC Adv.* **2020**, *10*, 8821–8824. [[CrossRef](#)]
17. Gagea, B.C.; Lorgouilloux, Y.; Altintas, Y.; Jacobs, P.A.; Martens, J.A. Bifunctional conversion of n-decane over HPW heteropoly acid incorporated into SBA-15 during synthesis. *J. Catal.* **2009**, *265*, 99–108. [[CrossRef](#)]
18. Llanos, A.; Melo, L.; Avendano, F.; Montes, A.; Brito, J.L. Synthesis and characterization of HPW/MCM-41 (Si) and HPW/MCM-41 (Si/Al) catalysts: Activity for toluene alkylation with 1-dodecene. *Catal. Today* **2008**, *133*, 20–27. [[CrossRef](#)]
19. Song, Y.X.; Xin, F.; Zhang, L.X.; Wang, Y. Oxidation of Cyclohexene in the Presence of Transition-Metal-Substituted Phosphotungstates and Hydrogen Peroxide: Catalysis and Reaction Pathways. *ChemCatChem* **2017**, *9*, 4139–4147. [[CrossRef](#)]
20. Domaille, P.J.; Hervéa, G.; Téazéa, A. Vanadium(V) Substituted Dodecatungstophosphates. In *Inorganic Syntheses*; Ginsberg, A.P., Ed.; Wiley: New York, NY, USA, 1990; Volume 27, Chapter 17; pp. 96–104.
21. Zhang, Z.; Huang, J.; Zhang, M.; Yuan, Q.; Dong, B. Ultrathin hexagonal SnS_2 nanosheets coupled with g- C_3N_4 nanosheets as 2D/2D heterojunction photocatalysts toward high photocatalytic activity. *Appl. Catal. B Environ.* **2015**, *163*, 298–305. [[CrossRef](#)]
22. Li, X.Y.; Ding, C.; Zhao, C.X.; Wang, F.; Li, C.L.; Yang, X.F. Activation of graphitic carbon nitride by solvent-mediated supramolecular assembly for enhanced hydrogen evolution. *Appl. Surf. Sci.* **2020**, *525*. [[CrossRef](#)]

23. Huang, J.; Liu, T.; Wang, R.; Zhang, M.; Wang, L.; She, H.; Wang, Q. Facile loading of cobalt oxide on bismuth vanadate: Proved construction of p-n junction for efficient photoelectrochemical water oxidation. *J. Colloid Interface Sci.* **2020**, *570*, 89–98. [[CrossRef](#)] [[PubMed](#)]
24. Wu, X.; Zhang, X.; Zhao, S.; Gong, Y.; Djellabi, R.; Lin, S.; Zhao, X. Highly-efficient photocatalytic hydrogen peroxide production over polyoxometalates covalently immobilized onto titanium dioxide. *Appl. Catal. A Gen.* **2020**, *591*, 117271. [[CrossRef](#)]
25. Dante, R.C.; Chamorro-Posada, P.; Vázquez-Cabo, J.; Rubiños-López, Ó.; Sánchez-árevalo, F.M.; Huerta, L.; Martín-Ramos, P.; Lartundo-Rojas, L.; ávila-Vega, C.F.; Rivera-Tapia, E.D. Nitrogen-carbon graphite-like semiconductor synthesized from uric acid. *Carbon* **2017**, *121*, 368–379. [[CrossRef](#)]
26. Wang, X.; Maeda, K.; Thomas, A.; Takanabe, K.; Xin, G.; Carlsson, J.M.; Domen, K.; Antonietti, M. A metal-free polymeric photocatalyst for hydrogen production from water under visible light. *Nat. Mater.* **2009**, *8*, 76–80. [[CrossRef](#)]
27. Ge, J.; Zhang, L.; Xu, J.; Liu, Y.; Jiang, D.; Du, P. Nitrogen photofixation on holey g-C₃N₄ nanosheets with carbon vacancies under visible-light irradiation. *Chin. Chem. Lett.* **2020**, *31*, 792–796. [[CrossRef](#)]
28. Zhu, Z.; Wang, B.; Yao, Q.; Zhou, Y.; Yang, H.; Liu, Y. H₃PW₁₂O₄₀/mpg-C₃N₄ as an efficient and reusable catalyst in the alkylation of o-xylene and styrene. *Appl. Organomet. Chem.* **2019**, *33*. [[CrossRef](#)]
29. Li, K.; Yan, L.; Zeng, Z.; Luo, S.; Luo, X.; Liu, X.; Guo, H.; Guo, Y. Fabrication of H₃PW₁₂O₄₀-doped carbon nitride nanotubes by one-step hydrothermal treatment strategy and their efficient visible-light photocatalytic activity toward representative aqueous persistent organic pollutants degradation. *Appl. Catal. B Environ.* **2014**, *156*, 141–152. [[CrossRef](#)]
30. Li, K.; Hu, J.; Li, W.; Ma, F.; Xu, L.; Guo, Y. Design of mesostructured H₃PW₁₂O₄₀-silica materials with controllable ordered and disordered pore geometries and their application for the synthesis of diphenolic acid. *J. Mater. Chem.* **2009**, *19*, 8628–8638. [[CrossRef](#)]
31. Lin, Z.; Wang, X. Nanostructure Engineering and Doping of Conjugated Carbon Nitride Semiconductors for Hydrogen Photosynthesis. *Angew. Chem. Int. Ed.* **2013**, *52*, 1735–1738. [[CrossRef](#)]
32. Li, X.-H.; Wang, X.; Antonietti, M. Solvent-Free and Metal-Free Oxidation of Toluene Using O₂ and g-C₃N₄ with Nanopores: Nanostructure Boosts the Catalytic Selectivity. *ACS Catal.* **2012**, *2*, 2082–2086. [[CrossRef](#)]
33. Pinto, T.; Arquilliere, P.; Dufaud, V.; Lefebvre, F. Isomerization of n-hexane over Pt-H₃PW₁₂O₄₀/SBA-15 bifunctional catalysts: Effect of the preparation method on catalytic performance. *Appl. Catal. A Gen.* **2016**, *528*, 44–51. [[CrossRef](#)]
34. Cao, S.-W.; Liu, X.-F.; Yuan, Y.-P.; Zhang, Z.-Y.; Liao, Y.-S.; Fang, J.; Loo, S.C.J.; Sum, T.C.; Xue, C. Solar-to-fuels conversion over In₂O₃/g-C₃N₄ hybrid photocatalysts. *Appl. Catal. B Environ.* **2014**, *147*, 940–946. [[CrossRef](#)]
35. Tian, B.; Tian, B.; Smith, B.; Scott, M.C.; Hua, R.; Lei, Q.; Tian, Y. Supported black phosphorus nanosheets as hydrogen-evolving photocatalyst achieving 5.4% energy conversion efficiency at 353K. *Nat. Commun.* **2018**, *9*, 1397. [[CrossRef](#)]
36. Pablo, M.-R.; Jesús, M.-G.; Manuela, R.S. Polymeric Carbon Nitride-Based Composites for Visible-Light-Driven Photocatalytic Hydrogen Generation. In *Hydrogen Production Technologies*; Scrivener Publishing: Beverly, MA, USA, 2017; pp. 579–621. [[CrossRef](#)]
37. Cao, S.-W.; Liu, X.-F.; Yuan, Y.-P.; Zhang, Z.-Y.; Fang, J.; Loo, S.C.J.; Barber, J.; Sum, T.C.; Xue, C. Artificial photosynthetic hydrogen evolution over g-C₃N₄ nanosheets coupled with cobaloxime. *Phys. Chem. Chem. Phys.* **2013**, *15*, 18363–18366. [[CrossRef](#)]
38. Guo, Y.; Li, K.; Yu, X.; Clark, J.H. Mesoporous H₃PW₁₂O₄₀-silica composite: Efficient and reusable solid acid catalyst for the synthesis of diphenolic acid from levulinic acid. *Appl. Catal. B Environ.* **2008**, *81*, 182–191. [[CrossRef](#)]
39. Lu, N.; Zhao, Y.H.; Liu, H.B.; Guo, Y.H.; Yuan, X.; Xu, H.; Peng, H.F.; Qin, H.W. Design of polyoxometallate-titania composite film (H₃PW₁₂O₄₀/TiO₂) for the degradation of an aqueous dye Rhodamine B under the simulated sunlight irradiation. *J. Hazard. Mater.* **2012**, *199*, 1–8. [[CrossRef](#)]
40. Svoboda, L.; Licciardello, N.; Dvorsky, R.; Bednar, J.; Henych, J.; Cuniberti, G. Design and Performance of Novel Self-Cleaning g-C₃N₄/PMMA/PUR Membranes. *Polymers* **2020**, *12*, 850. [[CrossRef](#)]
41. Niu, P.; Zhang, L.; Liu, G.; Cheng, H.-M. Graphene-Like Carbon Nitride Nanosheets for Improved Photocatalytic Activities. *Adv. Funct. Mater.* **2012**, *22*, 4763–4770. [[CrossRef](#)]

42. Wang, Q.; Wang, T.; Lv, Z.; Cui, M.; Zhao, Z.; Cao, X.; Wei, Q. TiO₂ Sol-Gel Coated PAN/O-MMT Multi-Functional Composite Nanofibrous Membrane Used as the Support for Laccase Immobilization: Synergistic Effect between the Membrane Support and Enzyme for Dye Degradation. *Polymers* **2020**, *12*, 139. [[CrossRef](#)]
43. Li, K.; Guo, Y.; Ma, F.; Li, H.; Chen, L.; Guo, Y. Design of ordered mesoporous H₃PW₁₂O₄₀-titania materials and their photocatalytic activity to dye methyl orange degradation. *Catal. Commun.* **2010**, *11*, 839–843. [[CrossRef](#)]
44. Wei, X.; Shao, C.; Li, X.; Lu, N.; Wang, K.; Zhang, Z.; Liu, Y. Facile in situ synthesis of plasmonic nanoparticles-decorated g-C₃N₄/TiO₂ heterojunction nanofibers and comparison study of their photosynergistic effects for efficient photocatalytic H₂ evolution. *Nanoscale* **2016**, *8*, 11034–11043. [[CrossRef](#)] [[PubMed](#)]
45. Song, K.; Xiao, F.; Zhang, L.; Yue, F.; Liang, X.; Wang, J.; Su, X. W₁₈O₄₉ nanowires grown on g-C₃N₄ sheets with enhanced photocatalytic hydrogen evolution activity under visible light. *J. Mol. Catal. A Chem.* **2016**, *418–419*, 95–102. [[CrossRef](#)]
46. Liu, J.; Liu, N.; Li, H.; Wang, L.; Wu, X.; Huang, H.; Liu, Y.; Bao, F.; Lifshitz, Y.; Lee, S. A critical study of the generality of the two step two electron pathway for water splitting by application of a C₃N₄/MnO₂ photocatalyst. *Nanoscale* **2016**, *8*, 11956–11961. [[CrossRef](#)] [[PubMed](#)]
47. Zhang, Z.; Liu, K.; Feng, Z.; Bao, Y.; Dong, B. Hierarchical Sheet-on-Sheet ZnIn₂S₄/g-C₃N₄ Heterostructure with Highly Efficient Photocatalytic H₂ production Based on Photoinduced Interfacial Charge Transfer. *Sci. Rep.* **2016**, *6*, 19221. [[CrossRef](#)]
48. Li, A.; Peng, Z.; Fu, X. Exfoliated, mesoporous W₁₈O₄₉/g-C₃N₄ composites for efficient photocatalytic H₂ evolution. *Solid State Sci.* **2020**, *106*, 106298. [[CrossRef](#)]
49. Yang, Y.; Mao, B.; Gong, G.; Li, D.; Liu, Y.; Cao, W.; Xing, L.; Zeng, J.; Shi, W.; Yuan, S. In-situ growth of Zn-AgIn₅S₈ quantum dots on g-C₃N₄ towards 0D/2D heterostructured photocatalysts with enhanced hydrogen production. *Int. J. Hydrogen Energy* **2019**, *44*, 15882–15891. [[CrossRef](#)]
50. Jin, X.; Fan, X.; Tian, J.; Cheng, R.; Li, M.; Zhang, L. MoS₂ quantum dot decorated g-C₃N₄ composite photocatalyst with enhanced hydrogen evolution performance. *RSC Adv.* **2016**, *6*, 52611–52619. [[CrossRef](#)]
51. Li, L.; Wu, Q.Y.; Guo, Y.H.; Hu, C.W. Nanosize and bimodal porous polyoxotungstate-anatase TiO₂ composites: Preparation and photocatalytic degradation of organophosphorus pesticide using visible-light excitation. *Microporous Mesoporous Mater.* **2005**, *87*, 1–9. [[CrossRef](#)]
52. Blanco, M.; Montaserin, C.; Angulo, A.; Perez-Marquez, A.; Maudes, J.; Murillo, N.; Aranzabe, E.; Ruiz-Rubio, L.; Vilas, J.L. TiO₂-Doped Electrospun Nanofibrous Membrane for Photocatalytic Water Treatment. *Polymers* **2019**, *11*, 747. [[CrossRef](#)]
53. Chen, S.; Zhang, M.Y.; Ma, X.Z.; Li, L.; Zhou, X.J.; Zhang, Z.Y. Asymmetric supercapacitors by integrating high content Na⁺/K⁺-inserted MnO₂ nanosheets and layered Ti₃C₂T_x paper. *Electrochim. Acta* **2020**, *332*, 135497. [[CrossRef](#)]

